Membrane Biology:

Cell Type-specific β2-Adrenergic Receptor Clusters Identified Using Photoactivated Localization Microscopy Are Not Lipid Raft Related, but Depend on Actin Cytoskeleton Integrity

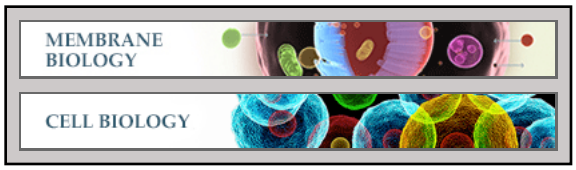

Marco Scarselli, Paolo Annibale and Aleksandra Radenovic

J. Biol. Chem. 2012, 287:16768-16780.
doi: 10.1074/jbc.M111.329912 originally published online March 22, 2012

THE JOURNAL OF BIOLOGICAL CHEMISTRY VOL. 287, NO. 20, pp. 16768–16780, May 11, 2012

Cell Type-specific β2-Adrenergic Receptor Clusters Identified Using Photoactivated Localization Microscopy Are Not Lipid Raft Related, but Depend on Actin Cytoskeleton Integrity*[S]

Received for publication, December 3, 2011, and in revised form, March 14, 2012 Published, JBC Papers in Press, March 22, 2012, DOI 10.1074/jbc.M111.329912

Marco Scarselli[1], **Paolo Annibale**[1], **and Aleksandra Radenovic**[2]

From the Laboratory of Nanoscale Biology, Institute of Bioengineering, School of Engineering, École Polytechnique Fédérale de Lausanne (EPFL), CH-1015 Lausanne, Switzerland

Background: The direct measurement of diffraction-limited structures, such as clusters, is outside the resolution of the available microscopy techniques.
Results: β2-Adrenergic receptor clusters identified using PALM are cell-type specific.
Conclusion: PALM has successfully allowed the quantitative determination of GPCR clusters.
Significance: The application of this powerful microscopy technique opens up the possibility to quantify the number of molecules in biological assemblies.

Recent developments in the field of optical super-resolution techniques allow both a 10-fold increase in resolution as well as an increased ability to quantify the number of labeled molecules visualized in the fluorescence measurement. By using photoactivated localization microscopy (PALM) and an experimental approach based on the systematic comparison with a nonclustering peptide as a negative control, we found that the prototypical G protein-coupled receptor β2-adrenergic receptor is partially preassociated in nanoscale-sized clusters only in the cardiomyocytes, such as H9C2 cells, but not in other cell lines, such as HeLa and Chinese hamster ovary (CHO). The addition of the agonist for very short times or the addition of the inverse agonist did not significantly affect the organization of receptor assembly. To investigate the mechanism governing cluster formation, we altered plasma membrane properties with cholesterol removal and actin microfilament disruption. Although cholesterol is an essential component of cell membranes and it is supposed to be enriched in the lipid rafts, its sequestration and removal did not affect receptor clustering, whereas the inhibition of actin polymerization did decrease the number of clusters. Our findings are therefore consistent with a model in which β2 receptor clustering is influenced by the actin cytoskeleton, but it does not rely on lipid raft integrity, thus ruling out the possibility that cell type-specific β2 receptor clustering is associated with the raft.

The results of some studies have led to the proposal that cell membrane proteins could be organized in signaling platforms, such as clusters or domains, to maintain the correct fidelity and efficacy in the transduction of the signal (1–3). Membrane compartmentalization resulting in signaling domains has been shown to occur through complex protein-protein, lipid-protein, and membrane-cytoskeletal interactions on the plasma membrane (1, 4). The concept of a lipid raft was the first to be introduced to biochemically explain the membrane heterogeneity. Lipid rafts are a well studied type of cholesterol- and sphingolipid-enriched, highly dynamic, membrane nanodomain, and numerous roles have been postulated for them (5, 6). For G protein-coupled receptors (GPCRs),[3] the largest family of membrane proteins, the existence and the role of protein clustering in relationship to the lipid rafts is still a controversial topic, and different indications have been provided on this matter (4, 7–9). Because cluster size is expected to lie below the diffraction limit, the use of conventional fluorescence microscopy is clearly not appropriate. Electron microscopy provides ultrastructural information at resolutions up to 1–2 nm, although the specific labeling by immune-gold antibodies of targeted proteins is not sufficient to quantify protein aggregates (10). To overcome such limitations, we applied one of the most promising optical super-resolution techniques, namely photoactivated localization microscopy (PALM), which improves the resolution up to 10 times with respect to conventional fluorescence microscopy and is able to determine the localization of single molecules with a precision of 10–20 nm (11, 12). The application of PALM is based on the serial photoactivation (or photoswitching) and subsequent bleaching of numerous sparse subsets of photoactivatable (or photoswitchable) fluorescent proteins (PA-FPs (or PS-FPs)). Operating PALM in total internal reflection fluorescence (TIRF) geometry is particularly advantageous for membrane receptors because it enhances the detection of fluorescent molecules within a thin layer of ~100 nm.

In previous research, some attempts to investigate spatial organization of membrane receptors have already been made. In the GPCR field, using atomic force microcopy, Fotiadis and

* This work was supported by Fonds National Suisse Grants 200021-125319 and 20021-132206.
[S] This article contains supplemental "Experimental Procedures" and Figs. S1–S7.
[1] Both authors contributed equally to this work.
[2] To whom correspondence should be addressed. E-mail: aleksandra.radenovic@epfl.ch.

[3] The abbreviations used are: GPCR, G protein-coupled receptor; PALM, photoactivated localization microscopy; TIRF, total internal reflection fluorescence; NSOM, near-field scanning optical microscopy; CCD, charge-coupled device; MβCD, methyl-β-cyclodextrin.

co-workers (13, 14) revealed that rhodopsin and opsin receptors are packed in ordered rows of dimers and oligomers that indicate a very dense level of receptor clustering. Atomic force microcopy is particularly suited for highly packed receptors in native cell membranes, such as rhodopsin and opsin, whereas its resolution can be severely affected in sparser samples. Another report, focusing on β1- and β2-adrenergic receptors in rat cardiac myocytes and HEK293 cells, used near-field scanning optical microscopy (NSOM) to show that the vast majority of receptors, detected via fluorescent antibodies, are imaged as clusters (7, 15). However, it is still technically challenging for NSOM to generate high spatial resolution images of plasma membrane proteins. This limitation stems from two sources: the first is that in NSOM the resolution is determined by the size of the aperture of the scanning optical fiber (typically in the range of 50–75 nm) and the second is the absence of highly photostable fluorophores.

In addition, as shown by Tanaka *et al.* (16), methods based on the use of primary and secondary antibodies are prone to artifacts arising from the clustering of the antibodies themselves. The authors demonstrated that the antibody-induced clustering could reach up to 66% of a membrane protein, the intrinsic clustering of which was rather low. In this respect, the use in PALM of photoactivatable-fluorescent proteins to label the target protein is clearly advantageous. Nevertheless, a careful approach is required when using PALM on structures, such as clusters, that can be identified only if the number of their constituents is known with a good precision (17). Moreover, to analyze protein aggregates properly, a negative control of a nonclustering peptide on the plasma membrane is an important requirement.

In this study, we investigated by PALM the membrane distribution of the prototypical GPCR β2-adrenergic receptor compared with the negative control of a nonclustering peptide. The constructs were labeled with the photoswitchable fluorophore mEos2 (18), which upon 405-nm laser light irradiation, converts irreversibly from green to red. It has been shown that accurate quantitative measurements can be performed using mEos2 to correctly image cell membrane clusters (17, 19). PALM experiments provide spatial point patterns made of the centers of emission of each localized fluorescent protein. These experiments were carried out in different cell lines, such as HeLa, CHO, and H9C2. We found that the β2-adrenergic receptor is partially preassociated in nanoscale-sized clusters only in H9C2 cells derived from the embryonic rat heart, but not in other cell lines. The addition of the agonist for very short times or the addition of the inverse agonist did not significantly affect receptor assembly.

Finally, we tried to interfere with β2-receptor clustering, altering membrane properties with cholesterol sequestration and removal, or actin microfilament disruption. Although cholesterol sequestration and removal did not influence the degree of receptor clustering, the inhibition of actin polymerization did decrease cluster formation.

EXPERIMENTAL PROCEDURES

DNA Constructs (Plasmids)—The *mEos2* gene cloned into the plasmid pRSETA was purchased from AddGene (Cambridge, MA) (AddGene plasmid 20341, original material provided by Loren Looger HHMI). The small peptide SrcN15 represents the N-terminal 15 amino acids of the protein Src, it is myristoylated (20) and was demonstrated to be associated with the nonraft domains of the plasma membrane. The two DNA constructs SrcN15-mEos2 and SrcN15-PSCFP2 were synthesized and cloned in the mammalian expression vector pJ603 by the DNA 2.0 Company (Menlo Park, CA). The company claims that the pJexpress mammalian vectors show equivalent levels of protein expression as pCDNA3.1 when using the same insert. When we compared the same construct present in two different vectors, pJ603 and pCDNA3.1, the expression level was similar (data not shown). All clones from DNA 2.0 were re-sequenced. The DNA construct of the N-terminal 10 amino acids of the protein Lck (LckN10) was synthesized by DNA 2.0 and then subcloned in the *SrcN15-mEos2* gene (vector pJ603) substituting the SrcN15 sequence with LckN10 using the unique restriction sites NotI and EcoRI. The small peptide LckN10 is myristoylated and palmitoylated and was demonstrated to reach the plasma membrane (20). For the β2-receptor chimera, we fused two different fluorophores tdEos and mEos2 (β2-tdEos and β2-mEos2) at the C terminus. For β2-tdEos, the β2 sequence was amplified with PCR using primers GATGAATTCCTTGGTACCACCATG (sense) and GGCGCGGCCGCTTCAGCAGTGAGTCATT (antisense) to obtain EcoRI and NotI restriction sites, and deletion of the Stop codon. Then, the amplified β2 construct was inserted in the plasmid for mammalian expression pcDNA3-td-Eos (from MoBiTec, 37083 Göttingen, Germany). For *β2-mEos2*, *mEos2* substitutes *tdEOS* in the *β2-tdEOS* DNA construct. The *mEos2* gene was amplified with polymerase chain reaction (PCR) using primers GTCGCGCTCGAGATGAGTGCGATTAAGCCA (sense) and CGTCGCGG-GCCCTTATCGTCTGGCATTGTC (antisense) to create XhoI and ApaI restriction sites. We decided to use *mEos2* fused to β2 because it is a monomer. For the constructs β2-PSCFP2 and M3-PSCFP2, we purchased the fluorophore PSCFP2 from Evrogen (Moscow, Russia) as pPS-CFP2-N for mammalian expression. We subcloned the *M3* construct at the N terminus of PSCFP2 amplifying with PCR *M3* sequence with primers CTTAAGCTTGGTACCACCATGTAC (sense) and CGCGGGCCCCCAAGGCCTGCTCGGG (antisense) to create EcoRI and ApaI restriction sites. A similar approach was made to subclone the β2 sequence in *PS-CFP2-N*, where the primers CTTAAGCTTGGTACCACCATGTAC (sense) and CGCGGGCCCCCAGCAGTGAGTCATT (antisense) were utilized. The clathrin-enhanced green fluorescent protein (EGFP) (light chain) construct was kindly given by Prof. Aurelien Roux (University of Geneva, Switzerland). mGFP-actin was purchased from AddGene (AddGene plasmid 21948).

Cell Cultures, Transfection, and Chemical Treatments—HeLa cells were purchased from ATCC (LGC Standards, Molsheim, France) and were grown in Dulbecco's modified Eagle's medium (DMEM) (without phenol red) supplemented with 10% fetal bovine serum, 100 mg/ml of streptomycin, and 100 units/ml of penicillin at 37 °C with 5% CO_2. The H9C2 cell line derived from the embryonic rat heart was from ATCC and was grown in DMEM (without phenol red) supplemented with 10% fetal bovine serum, 100 mg/ml of streptomycin, and 100

units/ml of penicillin at 37 °C with 5% CO_2. Both cell lines were transfected using the Neon™ Transfection System (Invitrogen, number 14072) following the manufacturer's instructions. Electroporation was performed in a 6-well dish (500,000–1,000,000 cells/well) using 0.5–2 μg of DNA for each sample following the manufacturer's parameters. For HeLa, the parameters for electroporation were 1,005 V and two pulses with a width of 35 ms. For H9C2, the parameters used were 1,650 V and three pulses with a width of 10 ms. After electroporation, the cells were seeded directly onto the coverslips. Experiments were performed 24 h after transfection. CHO (dihydrofolate reductase-deficient) cells were kindly provided by Dr. Jumhua Qiao (École Polytechnique Fédérale de Lausanne, Lausanne, Switzerland) and were grown in DMEM/F12, 1:1 (without phenol red), supplemented with 10% fetal bovine serum, 100 mg/ml of streptomycin, 100 units/ml of penicillin, and HT supplements at 37 °C with 5% CO_2 coverslips. For CHO, the parameters used for electroporation were 1,650 V and three pulses with a width of 10 ms. For cholesterol sequestration, we utilized filipin with a preincubation of 30 min at the concentration of 12 μg/ml, whereas for cholesterol removal we used MβCD preincubating for 30 min at 5 mM. For the internalization of β2-mEos2 in HeLa, cells were incubated at 37 °C in regular medium at different times with 10 μM isoproterenol (10 min was used as a reference time for internalization). The inhibitor of the clathrin-dependent endocytosis dynasore, at 80 μM, was preincubated for 30 min at 37 °C before internalization. For receptor activation, the incubation was only a few seconds (5 s was used as a reference time for receptor activation). After the experiment, samples were fixed using standard procedures (see sample fixation). Then, to assess the role of the actin cytoskeleton, we treated cells with 2 μM cytochalasin D, a actin polymerization inhibitor, preincubating the cells for 30 min. Isoproterenol hydrochloride, ICI 118,551 hydrochloride, filipin, cytochalasin D, and dynasore hydrate were purchased from Sigma.

cAMP Functional Assay—HeLa cells were electroporated with the specific DNA construct (β2, β2-mEos2, or β2-PSCFP2) for transient expression and were plated into 96-well plates at a density of 3 or 4×10^5 cells/well. On the day of the experiment (1 day after transfection), cells were preincubated in DMEM containing 20 mM HEPES (pH 7.4) and 0.1% albumin at 37 °C for 30 min in the presence of 10 μM rolipram, the phosphodiesterase inhibitor, to allow cAMP accumulation. Then, in the same buffer, the agonist isoproterenol was added at different concentrations for an additional 20 min. Receptor-mediated increases in intracellular cAMP were measured via the enzyme immunoassay method according to the manufacturer's protocol of the Amersham Biosciences cAMP enzyme immunoassay system (cAMP; Biotrak; GE Healthcare). After cell lysis for 15 min at room temperature with lysis solution, the supernatant from each sample was added to the specific 96-well plate from Amersham Biosciences coated with donkey anti-rabbit immunoglobulin G. Then, to measure the level of cAMP for each well, the samples were incubated subsequentially for 1 h with rabbit anti-cAMP antibody, the cAMP horseradish peroxidase, and, at the end, the enzyme substrate 3,3′,5,5′-tetramethylbenzidine. The assay is based on competition between unlabeled cAMP and a fixed quantity of peroxidase-labeled cAMP. A blue color develops at the end and the optical density (OD) can be read with the spectrophotometer plate reader at 630 nm. As an alternative, it is also recommended to stop the reaction with 1 M sulfuric acid and then read at 450 nm. To convert the change in OD at 450 nm into the amount of cAMP produced in the sample (fmol/well), a proper calibration curve done with the cAMP standards (12.5–3,200 fmol/well) was obtained.

Preparation of Supported Membrane Sheets—Following the protocol of Perez *et al.* (21), cells in a 6-well plate the day after transfection were washed three times with phosphate-buffered saline (PBS) and then covered with deionized water (pH 6–7) for 2 min to induce osmotic swelling. In the next step, a poly-L-lysine (0.1%)-coated coverslip was put on top of the cells for a few minutes and then removed, allowing the transfer of the membrane patches onto the glass coverslip. After rinsing the coverslip three times with PBS, the formed membrane sheets were fixed according to the protocol.

Sample Fixation—On the day of the experiment, the cells were incubated for 1 h in DMEM with no serum to purge them. Then, after extensive washing with PBS, cells were fixed by incubating with 4% paraformaldehyde and 0.2% glutaraldehyde at 37 °C for 30–60 min in PHEM (60 mM PIPES, 25 mM HEPES, 10 mM EDTA, and 2 mM $MgCl_2$, pH 6.9) and washed 5× with PHEM. The presence of glutaraldehyde was necessary to reduce molecule mobility as reported by Tanaka *et al.* (16). The glass coverslips were washed following the protocol of Shroff *et al.* (22). The coverslips (25.4 mm diameter, 1.5 thick) were cleaned overnight in a solution obtained by mixing 125 ml of water with 25 ml of ammonium hydroxide and 25 ml of 30% hydrogen peroxide. A further step based on repeated rinsing with MilliQ water, immersion in spectroscopic grade methanol, nitrogen blowing, and a passage under the flame was performed.

Cluster Analysis—Cluster analysis was performed on the localization maps provided by PALM images, by only retaining as members of a cluster those molecules with a density five times larger than the average density of the sample within a 150-nm radius. A filter on the localization precision was applied so that only those molecules localized to a precision better than 35 nm were included in the analysis. Clusters with fewer than five molecules were not included in the subsequent analysis. To avoid the effects arising from photoblinking being included in the analysis, a two-step approach was followed. Photoblinking refers to intermittent disappearance and reappearance of emitted light when molecules undergo reversible transitions between "on" and "off" states before they photobleach irreversibly. The first step consists of allowing a long dark period for each photoblinking molecule, effectively operating in an undercounting regime ($t_d = 10$ s). The second step is based on scoring the observed spatial clusters according to their degree of temporal clustering. This was performed by calculating, within a spatial cluster, the distance in time between the appearance of a molecule and that of the following one. The mean value of this distance in time was compared with that expected for a uniform distribution in time of the localization events. The ratio between these two values was used as a cluster score. Clusters

scoring poorly and therefore suggesting a photoblinking effect were discarded. As detailed in supplemental Fig. S1 all experimental data were divided into the following subgroups: HeLa or H9C2 cells expressing Src-N15 (negative control), cells expressing the β2 receptor (β2-mEos2 basal), cells expressing the β2 receptor and fixed after stimulation with the agonist isoproterenol (β2-mEos2 + Iso), and cells expressing the β2 receptor treated with agonist and the dynamin inhibitor dynasore (β2-mEos2 + Iso + Dyn). Cluster analysis was conducted after inspecting each cell and identifying a region of its cell membrane (an area of ~100 μm^2) lying as far as possible from the cell edge to minimize the "double layer" effect arising due to the folding of the plasma membrane within the TIRF excitation field. For the data presented in the color-coded Figs. 1*c*, 2, *c* and *f*, and 3, *c* and *f*, molecules were scored depending on their surrounding density, according to the formula,

$$L_i(r) = \sqrt{\frac{j(r)}{\pi}} - r \cdot \sqrt{\frac{N_{tot}}{A}}$$

where r represents the distance from the ith molecule, $j(r)$ the number of molecules within a circle of radius r centered on i, N_{tot}, and A represent the total number of molecules and area of the investigated region, respectively. $L_i(r)$ was estimated at a value of $r = 150$ nm.

Comparison of the degree of clustering using the function $L(r) - r$: Ripley's K test provides a quantitative indication of the deviations of the observed spatial point pattern from a random distribution. It also provides information about the length scale where such deviations occur. The function $L(r) - r$ is derived from Ripley's K function according to Ref. 23,

$$L(r) - r = \sqrt{\frac{K(r)}{\pi}} - r$$

where $L(r)$ displays the magnitude of deviations from a random distribution as positive y values. A completely random distribution of the observed pattern would yield a $L(r) - r$ value equal to 0. For a given number of particles in an area, 99% confidence intervals for the random distribution are constructed, running a large number of simulations of a random pattern. The experimental curves in Figs. 4*i* and 5*g* are normalized so that $L(r) - r = 1$ for the random spatial distribution. Data analysis was performed using (Wavemetrics, Lake Oswego, Portland, OR) IgorPro and custom-written routines.

Equipment and Settings—The excitation setup, built on an independent optical platform, consists of three laser-diode lines, two for excitation (488 nm Coherent (Santa Clara, CA) Sapphire 488-50 and 561 nm Spectra-Physics Excelsior) and one for photoactivation (405 nm Coherent Cube). The excitation light is amplitude modulated and gated through an acousto-optical polychromatic tunable filter (AOM) (A.A. Optoelectronics, Cedex, France), which allows an on-off switching of each line with a rise time of 1.5 ms. Both the excitation and activation beams are expanded (15–20 times) and the activation beam is spatial filtered (pinhole size, 10 μm). The filtered and expanded activation beam is combined to the excitation beam-path by a Semrock (New York) R405-Di01 dichroic mirror. The combined laser beams are focused to the back focal plane of a 1.45 NA ×100 Olympus TIRF objective by a 250-mm focal length, 50-mm diameter, achromatic doublet lens placed on a *x-y-z* micrometric translation stage. Total internal reflection at the sample arises as the focused laser beam is translated away from the optical axis in the back focal plane of the objective, resulting in a controllable exit angle of the beam with respect to the optical axis. In our setup, the beam angle is accurately controlled by the rotation of a 9.5-mm thick fused silica laser grade window (SQW-2037-UV Melles Griot (Albuquerque, NM)) placed on a rotating goniometer. The goniometer is mounted between the achromatic doublet and the back focal plane of the objective. The microscope is based on the structure of an inverted Olympus model IX 71, with a camera side-port and excitation port at the rear of the frame. Excitation and fluorescent wavelengths are separated by a Semrock FFT506Di02 dichroic mirror (PSCFP2) or a Chroma T585LP (mEos2), and a Chroma (Bellows Falls, VT) ET 525/50 (PSCFP2) or a Semrock FF01–617/73 (mEos2) are used as emission filters. Single-molecule fluorescence images are detected by an Andor Technology (Belfast, Ireland) iXon+ DU-897E electron multiplying charge-coupled device (CCD) camera, after a 2× (or 1.2×) further magnification, yielding a pixel size of 80 nm (or 133 nm). Custom-developed LabView (National Instruments) software controls the PALM acquisition sequence, triggering the CCD detector at each excitation cycle. The CCD detector, in turn, has the possibility to trigger the AOM, to avoid any stray light on the CCD chip and therefore bleed-through during readout. Data are spooled to the hard drive for post-processing. The 561-nm excitation power, as measured in epifluorescence mode after the objective, resulted in power densities at the sample in the range of 250–1000 W/cm^2. Datasets were recorded by reaching to both ends of this power range. For both mEos2 and PSCFP2, we used activation powers at 405 nm in the range of 10–100 milliwatts/cm^2.

PALM Image Acquisition—Single molecules were localized and rendered using MATLAB (MathWorks, Inc., Natick, MA) code kindly provided by Dr. Eric Betzig and the resulting spatial point patterns were analyzed with IgorPro custom routines.

The PALM image from a stack of 59,000 × 10-ms exposure time frames, 16-bit image depth, as shown in Fig. 1*a*, used an Olympus 60 × 1.45 NA objective + 2× additional magnification yielding a pixel size of 133 nm. Imaging was at room temperature (RT) in PHEM medium. Chroma T585LP and Semrock FF01-617/73 were used. The PALM pixel size is 8 nm; and the PALM pixel size in the inset is 3 nm (Fig. 1*b*). Only molecules localized to better than 35 nm are displayed. Fig. 2, *a* and *b*, show the PALM image from a stack of 70,000 × 50-ms exposure time frames, 16-bit image depth. Olympus 60 × 1.45 NA objective + 2x additional magnification yielding a pixel size of 133 nm was used with imaging at RT in PHEM medium. Chroma T585LP and Semrock FF01-617/73 were used. PALM pixel size is 8 nm and PALM pixel size in the inset is 3 nm (Fig. 2*b*). Only molecules localized to better than 35 nm are displayed.

Fig. 2, *d* and *e*, show the PALM image from a stack of 450,000 × 10-ms exposure time frames, 16-bit image depth.

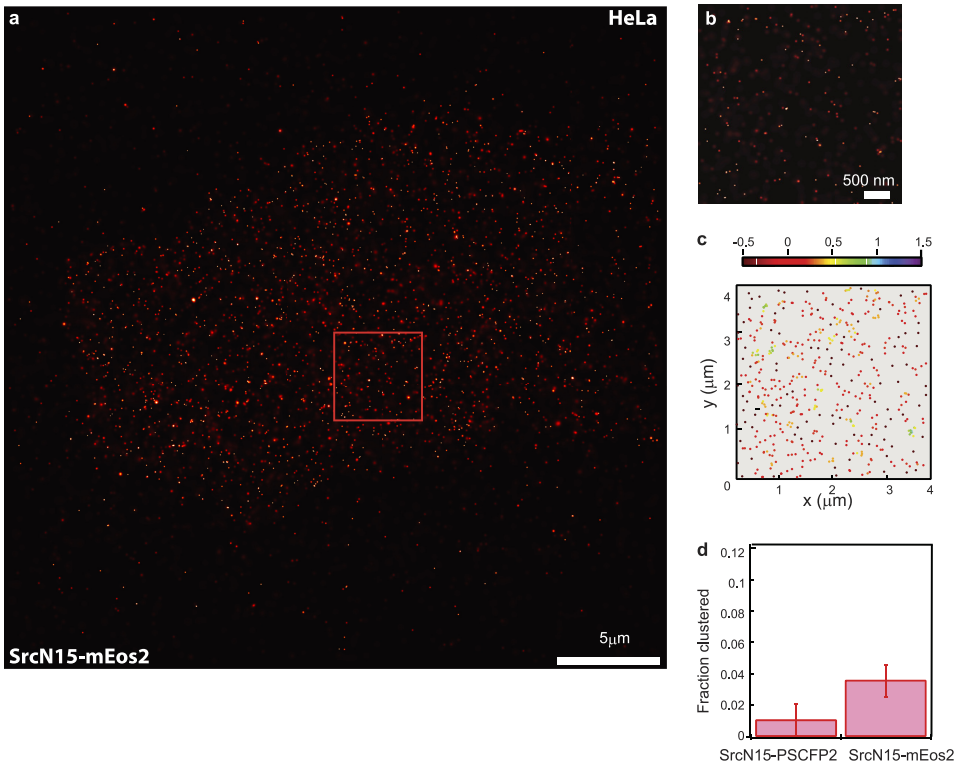

FIGURE 1. **PALM image of the nonclustering peptide SrcN15-mEos2 on the plasma membrane of HeLa cells.** *a*, PALM image in TIRF fluorescence geometry of a small peptide of 15 amino acids of the protein Src (the nonclustering peptide SrcN15-mEos2) on the plasma membrane of fixed HeLa cells. Images that are shown are representative of experiments that were repeated at least five times. *b,* magnified view of *boxed region* in *a*. *c,* schematic representation of the molecule distribution of the *inset in a* to visualize clusters (different colors represent clustering degree). *d,* quantification of the fraction clustered of the nonclustering peptide (negative control) labeled with two different fluorophores, SrcN15-mEos2 and SrcN15-PSCFP2. The bar graph shows the fraction clustered as the average ± S.E.

Olympus 100 × 1.45 NA objective + 2× additional magnification yielding a pixel size of 80 nm was used with imaging at RT in PHEM medium. Chroma T585LP and Semrock FF01-617/73 were used. The PALM pixel size is 5 nm; PALM pixel size in the inset is 3 nm (Fig. 2*e*). Only molecules localized to better than 35 nm are displayed.

Fig. 3, *a* and *b,* show the PALM image (Fig. 3*a*) from a stack of 29,000 × 50 ms exposure time frames, 16-bit image depth with an Olympus 60 × 1.45 NA objective + 2x additional magnification yielding a pixel size of 133 nm with imaging at RT in PHEM medium. Chroma T585LP and Semrock FF01-617/73 were used. The PALM pixel size is 8 nm; the PALM pixel size in the inset is 3 nm (Fig. 3*b*). Only molecules localized to better than 35 nm are displayed. In Fig. 3, *d* and *e,* the PALM image from a stack of 21,000 × 50 ms exposure time frames, 16-bit image depth with an Olympus 60 × 1.45 NA objective + 2x additional magnification yielding a pixel size of 133 nm was used. Imaging was at RT in PHEM medium. Chroma T585LP and Semrock FF01-617/73 were used. PALM pixel size is 8 nm; PALM pixel size in the inset is 3 nm (Fig. 3*e*). Only molecules localized to better than 35 nm are displayed.

Fig. 4, *a* and *b,* show the PALM image (Fig. 4*a*) from a stack of 30,000 × 50-ms exposure time frames, 16 bit image depth on a Olympus 60 × 1.45 NA objective + 2× additional magnification yielding a pixel size of 133 nm and PALM image (*b*) from a stack of 25,000 × 50-ms exposure time frames, 16-bit image depth on an Olympus 100 × 1.45 NA objective + 2× additional magnification yielding a pixel size of 80 nm. PALM Pixel size is 3 nm with imaging at RT in PHEM medium. Chroma T585LP and Semrock FF01-617/73 were used. Only molecules localized to better than 35 nm are displayed.

Fig. 5, *a* and b, are PALM images from a stack of 40,000 × 50-ms exposure time frames, 16-bit image depth on a Olympus 100 × 1.45 NA objective + 2× additional magnification yielding a pixel size of 80 nm. Imaging was at RT in PHEM medium. Chroma T585LP and Semrock FF01-617/73 were used. PALM pixel size is 5 nm. Only molecules localized to better than 35 nm are displayed.

Plasma Membrane Distribution in HeLa Cells of the Nonclustering Short Peptide SrcN15 Using PALM—For proper identification of receptor clustering, a negative control of a nonclustering peptide on the plasma membrane is an important starting point. To this purpose, we used a small peptide of 15 amino acids of the N terminus of the Src protein (SrcN15) that is myristoylated and has been shown to reach the plasma membrane (20, 25). For the quantitative determination of the clustered fraction, molecules with a surrounding local density exceeding five times the average molecular density were considered as being part of a cluster according to Ripley's method (23, 26). Aggregates with fewer than five molecules or identified as originating from photoblinking were discarded as detailed in the supplemental "Experimental Procedures". The ratio between the molecules being part of a cluster and the total number of localized molecules yielded the clustering fraction. The small protein fragment SrcN15 was labeled with mEos2 (SrcN15-mEos2) and the PALM images were taken in TIRF

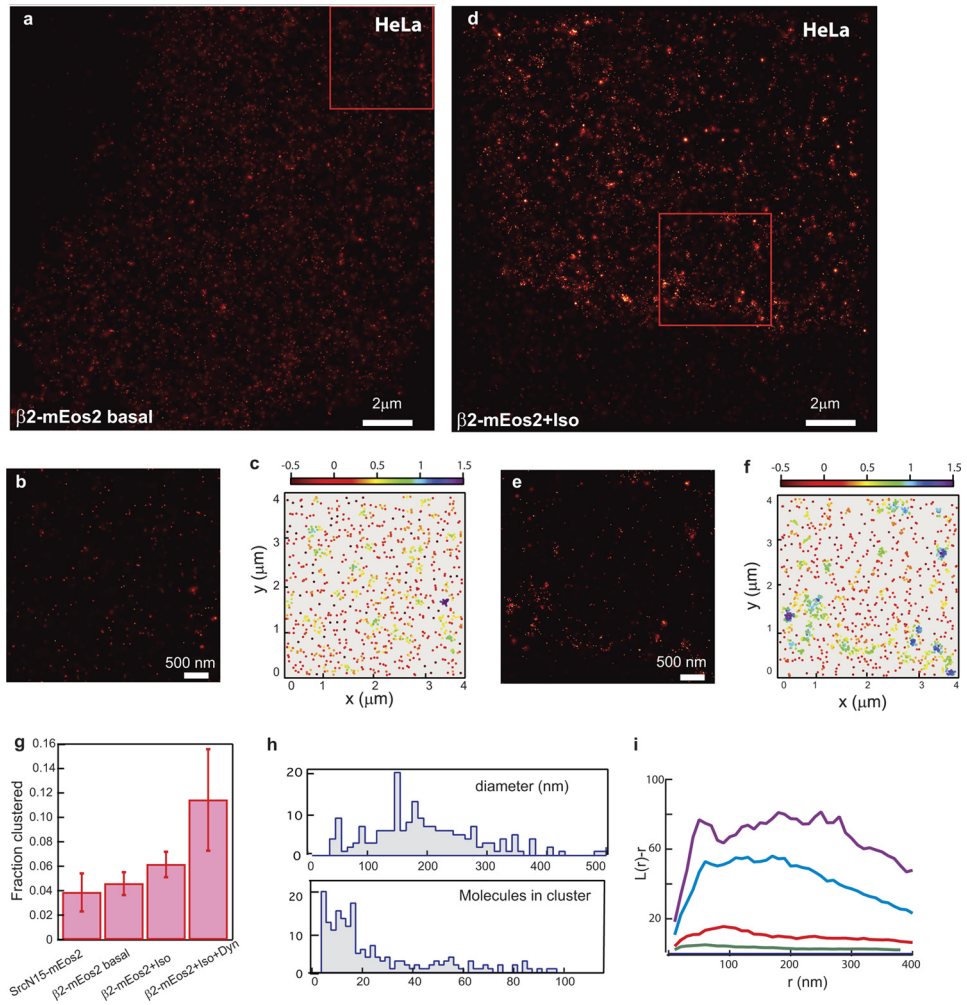

FIGURE 2. **PALM images and cluster analysis of the β2 receptor labeled with mEos2 (β2-mEos2) on the plasma membrane of HeLa cells before and after agonist addition.** *a,* PALM image in TIRF geometry of β2-mEos2 in basal conditions on the plasma membrane of fixed HeLa cells. Images that are shown are representative of experiments that were repeated at least five times. *b,* magnified view of *boxed region* in *a*. *c,* schematic representation of the molecule distribution of the *inset* to visualize clusters (different colors represent clustering degree). *d*, PALM image in TIRF geometry of β2-mEos2 on the plasma membrane of fixed HeLa cells after incubation with the agonist (isoproterenol 10 μM, 10 min) during endocytosis. Images that are shown are representative of experiments that were repeated at least five times. *e,* magnified view of *boxed region* in *d*. *f,* schematic representation of the molecule distribution of the inset to visualize clusters. *g,* quantification of the clustered fraction in HeLa of the β2-mEos2 basal state, β2-mEos2 + Iso (isoproterenol 10 μM, 10 min), β2-mEos2 + Iso + Dyn (dynasore 80 μM) compared with the negative control (the nonclustering peptide SrcN15-mEos2). Dynasore is an inhibitor of clathrin-dependent endocytosis. The bar graph shows the fraction clustered as the average ± S.E. *h*, *bottom,* histogram representing the distribution of the number of molecules present in the clusters (Events) of β2-mEos2 during endocytosis in the presence of agonist (isoproterenol 10 μM, 10 min) and dynasore 80 μM. *Top*, histogram representing the distribution of the cluster diameter size of β2-mEos2 during endocytosis in the presence of agonist (isoproterenol 10 μM, 10 min) and dynasore 80 μM. *i,* the degree of clustering for the experiments was determined by Ripley's *K* function analysis and $L(r) - r$ parameter that displays the magnitude of deviations from a random distribution as positive *y* values (normalized to 99% confidence interval). Data are representative of experiments that were repeated at least three times. SrcN15-mEos2 (*green curve*), β2-mEos2 basal state (*red curve*), β2-mEos2 + Iso (*blue curve*), β2-mEos2 + Iso + Dyn (*violet curve*) are indicated.

geometry to visualize the protein expressed on the plasma membrane.

In HeLa cells, the negative control SrcN15-mEos2 was randomly distributed all over the plasma membrane after fixation, and the clustering fraction was less than 4% (Fig. 1, *a* and *b*). The map of the localized centers of emission (in Fig. 1*c* color coded for the degree of clustering) shows how most of the molecules are localized as monomers. A low clustering fraction was also obtained when a different photoswitchable fluorophore was used to label SrcN15, SrcN15-PSCFP2 (less than 2%, Fig. 1*d*), or when another small peptide containing the N-terminal 10 amino acids of the protein Lck was used (LckN10-mEos2) (data not shown). We decided to use mEos2 as a fluorophore label throughout our study because it is brighter than PSCFP2 and thus allows a better localization precision.

Cluster Analysis of β2-Adrenergic Receptor on Plasma Membrane of HeLa Cells before and after Agonist Addition—Next, we analyzed the clustering fraction of the β2 receptor labeled with mEos2 (β2-mEos2) in HeLa cells. The construct was correctly expressed and it proved to be functional as the wild-type receptor (supplemental Fig. S2). In the basal state, the average clustering fraction of β2-mEos2 was about 4% after fixation, not different from the negative control (Fig. 2, *a*-c). After the addition of the agonist isoproterenol (10 μM) for 5 s, immediately before fixation, the average clustering of the receptor did not appear to change with respect to the basal state (data not

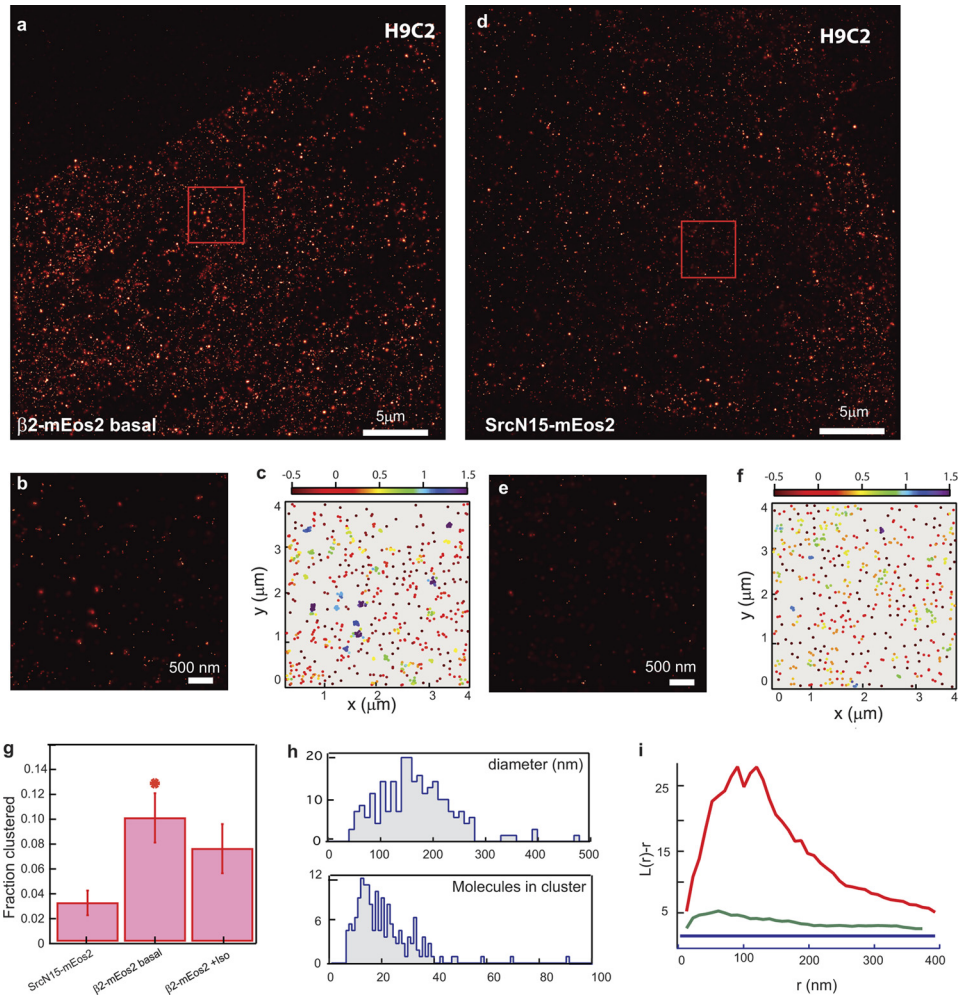

FIGURE 3. **PALM images and cluster analysis of β2-mEos2 on the plasma membrane of the H9C2 cell line derived from embryonic rat heart.** *a*, PALM image in TIRF geometry of β2-mEos2 in basal conditions on the plasma membrane of fixed H9C2 cells. Images that are shown are representative of experiments that were repeated at least five times. *b*, magnified view of *boxed region* in *a*. *c*, schematic representation of the molecule distribution of the inset to visualize clusters (different colors represent clustering degree). *d*, PALM image in TIRF geometry of the nonclustering peptide SrcN15-mEos2 on the plasma membrane of fixed H9C2 cells. Images that are shown are representative of experiments that were repeated at least five times. *e*, magnified view of *boxed region* in *d*. *f*, schematic representation of the molecules distribution of the inset to visualize clusters. *g*, quantification of the fraction clustered of the negative control SrcN15-mEos2, β2-mEos2 in basal conditions, and β2-mEos2 in the presence of the agonist for very short times (10 μM isoproterenol, 5 s). The bar graph shows the fraction clustered as the average ± S.E. (*, $p = 0.0023$; one-tailed test). *h*, *bottom,* histogram representing the distribution of the number of molecules present in the cluster of β2-mEos2 in basal conditions. *Top,* histogram representing the distribution of the cluster diameter size of β2-mEos2 in basal conditions. *i*, the degree of clustering for the experiments was determined by Ripley's *K* function analysis and $L(r) - r$ parameter that displays the magnitude of deviations from a random distribution as positive *y* values (normalized to 99% confidence interval). Data are representative of experiments that were repeated at least three times. SrcN15-mEos2 (*green curve*) and β2-mEos2 basal state (*red curve*) are indicated.

shown). At a longer incubation with the agonist, the clustered fraction displayed a slight increase with respect to the basal state, in agreement with the receptor being internalized. The increase in the clustering fraction was reinforced by the addition of the inhibitor of the clathrin-dependent endocytosis, dynasore at 80 μM (Fig. 2*g*). Even if we observed a clear trend in the increase in the clustering fraction in the presence of the agonist at 10 min (particularly adding dynasore) compared with the basal state, the difference was not statistically significant (Fig. 2*g*). This was probably due to the variability of the internalization process in the presence of dynasore, the sparse number of the forming endosomes, the peculiarity of the approach used, and the variability in receptor density from cell to cell, as discussed in supplemental "Experimental Procedures" and Fig. S1. Even in diffraction-limited TIRF experiments observing cell membrane receptors undergoing endocytosis, the number of cluster features appeared to be sparse and in the ~0.2–0.3/μm^2 range (25). However, the Ripley *L* function analysis confirms in Fig. 2*g* the presence of an increased degree of clustering during receptor endocytosis. We confirmed that receptor clusters corresponded to forming endosomes by colocalization experiments between clathrin-EGFP and the β2-mEos2 receptor after 10 min of isoproterenol (supplemental Fig. S3). A similar experiment of colocalization between the GPCR during endocytosis and the clathrin-coated pit was previously reported by Puthenveedu and von Zastrow (25). Detailed information about receptor clusters during endocytosis, such as clustering fraction, size, and number of molecules present in the clusters, is shown in Fig. 2, *h* and *i*. Receptor expression on the plasma membrane ranged from 10 to 160 molecules/μm^2 with an average value of at least 59 molecules/μm^2 and a median value of at least 43 molecules/μm^2. These values compare well with those previously estimated for the endoge-

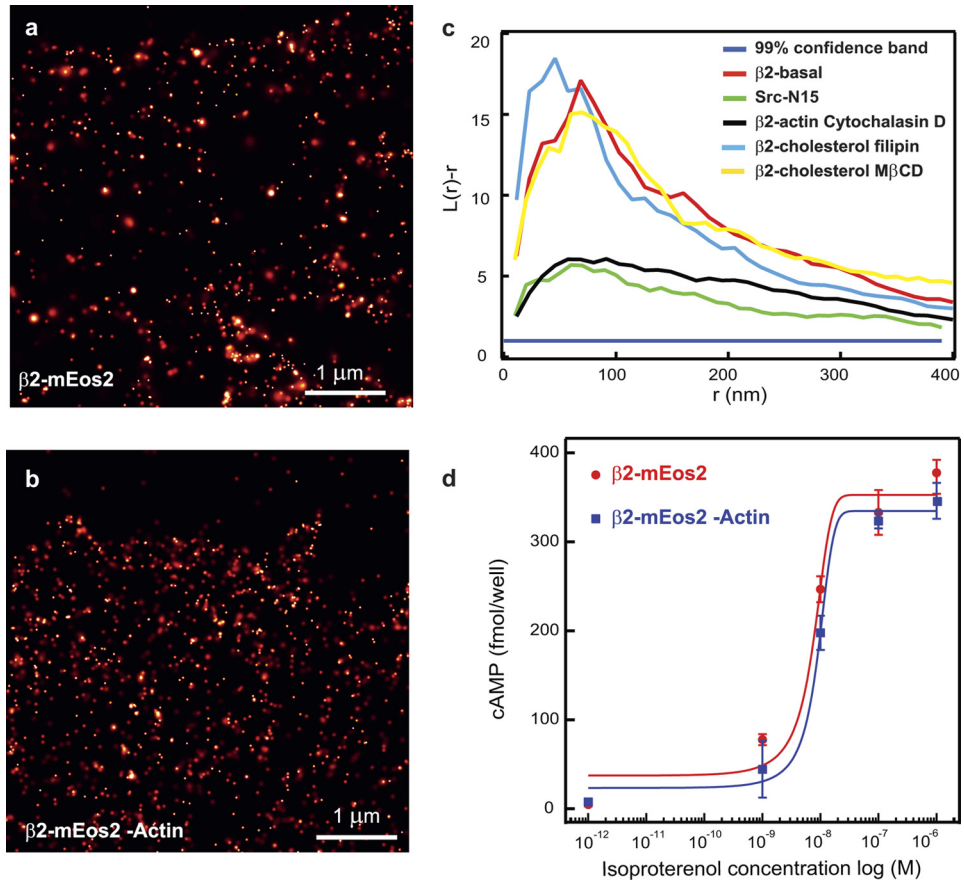

FIGURE 4. **PALM images and cluster analysis of β2-mEos2 on the plasma membrane of H9C2 cells after cholesterol sequestration or actin microfilament disruption.** *a* and *b*, PALM images in total internal reflection fluorescence geometry of β2-mEos2 on the plasma membrane of fixed H9C2 cells in basal condition (*a*), and after actin cytoskeleton disruption (*b*). *c*, the degree of clustering for the experiments shown was determined by Ripley's *K* function analysis and $L(r) - r$ parameter that displays the magnitude of deviations from a random distribution as the positive *y* values (normalized to 99% confidence interval). Data are representative of experiments that were repeated at least three times. Cholesterol inactivation was obtained by preincubating cells with filipin for 30 min at the concentration of 12 μg/ml or MβDC with a preincubation of 30 min at 5 mM, whereas actin microfilament disruption was performed by preincubating for 30 min with cytochalasin D at 2 μM. *d*, concentration-response curve in the cAMP accumulation assay in H9C2 cells expressing β2-mEos2 in the presence of cytochalasin D (β2-mEos2-actin, *blue curve*) or β2-mEos2 without cytochalasin D (β2-mEos2, *red curve*). The EC_{50} resulted in 7.10 ± 1.51 and 8.74 ± 0.74 nM, respectively. These data are representative of three different experiments.

nous β2 receptor in myocytes and A549 cells, namely 30 and 20/μm^2, respectively (27, 28). It is worthwhile mentioning that HeLa cell morphology was not particularly affected by cell transfection with our constructs (data not shown).

Our results proved the absence of clusters of the β2 receptor in HeLa cells in the steady state and at the moment of receptor activation after addition of the agonist for very short times. The same evidence was found in the CHO cell line, where the β2-mEos2 clustering fraction in the basal state was only about 2% (data not shown). In CHO cells, the presence of the endogenous β2 receptor is negligible (29), whereas in HeLa cells, the amount of β2 is rather low (30). Considering that we looked for clusters of at least five molecules, we cannot exclude the presence of receptor oligomers (or dimers) in these conditions. A control based on another GPCR in HeLa cells, namely M3 muscarinic receptor, demonstrated that the clustered fraction of M3 muscarinic construct, M3-PSCFP2, was negligible as shown for the β2 receptor (supplemental Fig. S4).

Cluster Analysis of β2-Adrenergic Receptor on Plasma Membrane of Cardiomyocytes, Such as H9C2 Cells, before and after Agonist Addition—To further examine the presence of β2 receptor clusters in other cell types, we decided to consider the H9C2 cell line derived from embryonic rat heart. In H9C2 cells, the expression and functional role of the endogenous β2 receptor have been extensively studied and well characterized (31, 32).

PALM measurements allowed us to visualize a certain degree of β2 receptor clustering already in the basal state (Fig. 3, *a-c*) after fixation. The clustering fraction was about 10%, whereas the negative control reached only 3% of clustering (Fig. 3, *d-f*). We have observed an expression level of β2-mEos2 ranging from only a few to 150 molecules/μm^2. This is a range that covers an expression level close to physiological conditions and up to amounts generally found in heterologous systems. We could not observe a significant increase in the number of clusters or an increase in the clustered fraction as a function of the expression level. Receptor expression displayed an average value of at least 67 molecules/μm^2 and a median value of at least 47 molecules/μm^2, and the effect of the expression level on the experimental findings is shown in supplemental Fig. S1. PALM images yielded a number of β2 cluster features in the ~0.1–0.2/μm^2 range, which compares with ~1–1.4/μm^2 from previous NSOM data (7, 15). The presence of the endogenous β2 receptor in H9C2 cells in the clustered fraction, undetected by

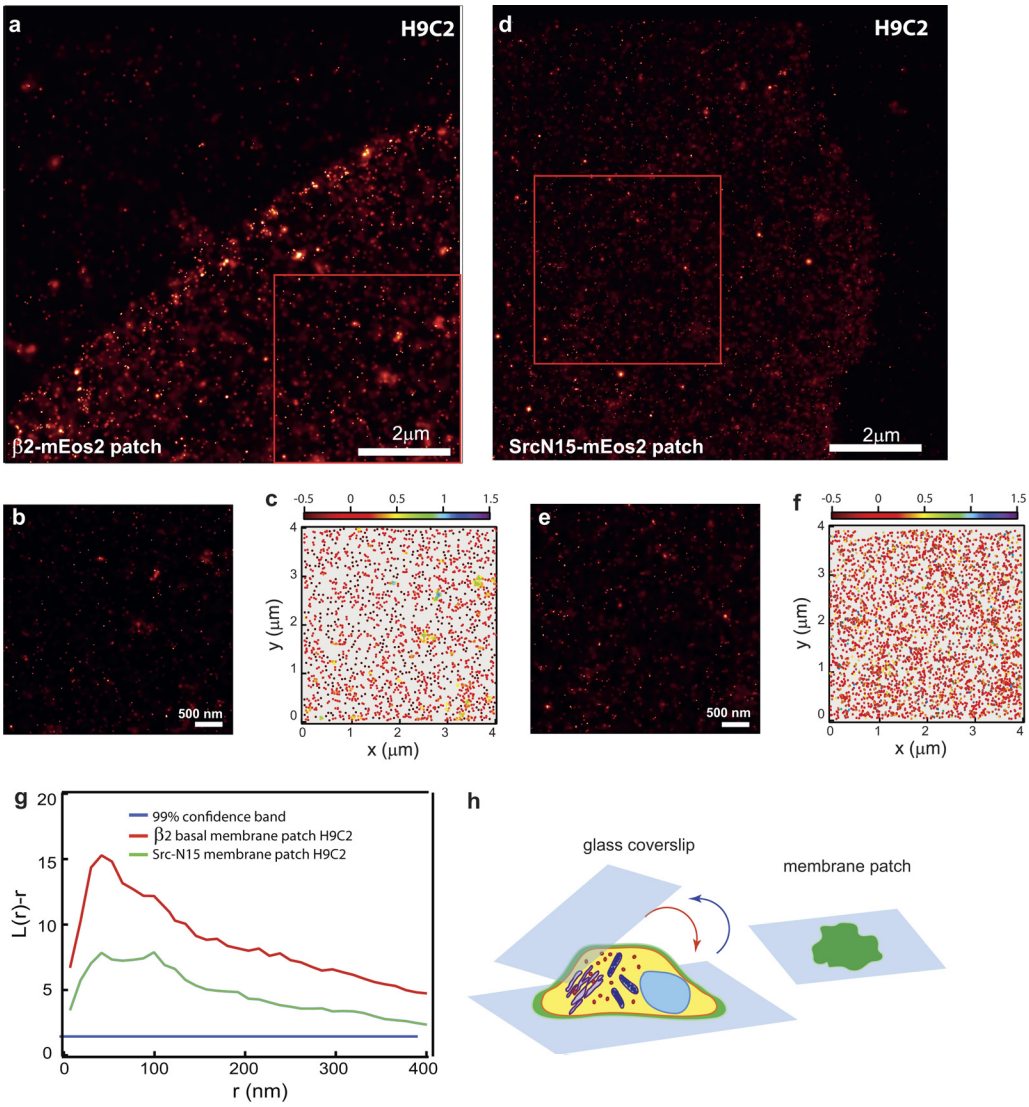

FIGURE 5. **PALM images and cluster analysis of β2-mEos2 and nonclustering peptide SrcN15-mEos2 on supported cell-membrane sheets of H9C2 cells.** *a,* PALM image in TIRF geometry of β2-mEos2 in basal conditions on H9C2 membrane sheets obtained by transferring plasma membrane onto poly-L-lysine-coated coverslips and then fixing. Images are representative of experiments that repeated at least three times. *b,* magnified view of *boxed region* in *a*. *c,* schematic representation of the molecule distribution of the *inset* to visualize clusters (different colors represent clustering degree). *d,* PALM image in TIRF geometry of the nonclustering peptide SrcN15-mEos2 on H9C2 membrane sheets obtained using the same condition as in *a*. *e,* magnified view of *boxed region* in *d*. *f,* schematic representation of the molecule distribution of the *inset* to visualize clusters. *g*, the degree of clustering for β2-mEos2 and SrcN15-mEos2 was determined by Ripley's *K* function analysis and $L(r) - r$ parameter that displays the magnitude of deviations from a random distribution as positive *y* values (normalized to 99% confidence interval). Data are representative of experiments that were repeated at least three times. *h,* schematic representation of the experimental procedure used to obtain the membrane sheets (patches) onto poly-L-lysine-coated coverslips. Following the protocol of Perez *et al.* (21), a poly-L-lysine-coated coverslip was put on top of the cells for few minutes and then removed allowing the transfer of the membrane patches onto the glass coverslip.

PALM, can lead to an underestimation in our data of the real clustering fraction. However, the immunofluorescence images (supplemental Fig. S5) and the PALM data comparing the expression of the exogenous β2 receptor suggest that the impact of the endogenous β2 receptor on the cluster analysis is limited. Importantly, when the full agonist isoproterenol was added for 5 s, the clustering fraction of the β2 receptor in H9C2 cells was not significantly affected (Fig. 3*g*). These observations suggest that if the partial receptor clustering in H9C2 is relevant, in certain aspects, for receptor signaling, this assembly is already preassociated before the addition of the ligand. The confirmation of the specificity of β2-mEos2 clusters in H9C2 cells comes from the fact that we did not find any clustering of M3 receptor expressed in the same cells as shown in supplemental Fig. S4. Finally, when the inverse agonist ICI 118,551 (33) was added (1 μM) to the β2 receptor in H9C2 cells, the clustering fraction of β2 in H9C2 cells was still not significantly affected (data not shown), ruling out the possibility of receptor basal activity as the main cause for the formation of the clusters.

Cluster Analysis of β2-Adrenergic Receptor on Plasma Membrane of H9C2 Cells after Cholesterol Sequestration or Actin Microfilament Disruption—To investigate the mechanism governing β2 receptor clustering in H9C2 cells, we tried to interfere with this phenomenon altering membrane properties. In particular, we looked to see if cholesterol played a role in receptor clustering. Cholesterol is an essential component of mam-

malian cell membranes and plays a crucial role in membrane organization (34). In particular, it has been postulated that the existence of cholesterol-rich liquid-ordered lipid domains, the "lipid rafts," can act as membrane anchors for signaling molecules and induce protein aggregation, such as clustering (35). Interestingly, a recent study reported that cholesterol can modulate GPCR functional properties through a specific direct interaction (36). The sequestration of cholesterol and the consequent modification of the lipid raft properties can be realized through different chemicals, such as methyl-β-cyclodextrin (MβDC) or filipin. If MβDC rapidly extracts cholesterol from the plasma membrane and disrupts the lipid raft, filipin binds and selectively sequesters cholesterol, only modifying raft properties (37). However, the use of MβDC, a stronger approach for cholesterol sequestration, causes more side effects due to its pleiotropic properties (38–40). For this reason, we decided to utilize both cholesterol-altering agents, filipin with a preincubation of 30 min at the concentration of 12 μg/ml and MβDC with a preincubation of 30 min at the concentration of 5 mM. The acute addition of both treatments did not change the assembly of the β2 receptor, indicating that receptor clustering does not rely on lipid raft integrity and thus ruling out the possibility that β2 cluster formation is associated with the raft (Fig. 4). The receptor clustering was determined by Ripley's *K* function analysis and $L(r) - r$ curves display the magnitude of deviations from a random distribution as positive *y* values (Fig. 4*c*). If cholesterol has a very important role in plasma membrane properties, the actin cytoskeleton is also relevant for lateral diffusion of membrane lipids and proteins. The actin cytoskeleton lies immediately below the plasma membrane and it has been shown, together with other cytoskeleton intermediates, to impose constraints on the mobility of membrane proteins. Recent studies demonstrated that the actin cytoskeleton destabilization affects GPCR signaling (41–43). To assess the role of the actin cytoskeleton, we treated H9C2 cells with 2 μM cytochalasin D, preincubating cells for 30 min. The clustering of β2 receptor, as indicated by the $L(r) - r$ function, was clearly reduced by the actin-disrupting chemical (Fig. 4*c*). This implies an important role of the actin cytoskeleton in receptor assembly that is not associated with the lipid raft. Neither treatment altered the morphology of most of the cells, even if a minority suffered in these conditions (data not shown).

To place these observations in a physiological context, we performed the cAMP functional assay after actin depletion in H9C2 cells expressing β2-mEos2. Actin depletion did not significantly affect the production of cAMP when it was measured in the cellular bulk after incubation with the agonist for 10 min (Fig. 4*d*). However, this kind of bulk test most likely misses fine changes that can be related to a receptor clustering within nanosized domains.

Cluster Analysis of β2-Adrenergic Receptor on Supported Cell-Membrane Sheets of H9C2 Cells—Considering that receptor clustering is a biological process related to the plasma membrane, we decided to use a different biological condition where we obtained functional supported cell-membrane sheets on poly-L-lysine-coated coverslips. Cell-membrane sheets can be prepared by detachment of the plasma membrane of living cells that are transferred to a poly-L-lysine-coated glass coverslip as observed by Perez *at al.* (21). These membranes maintain most of their functional properties as in the native conditions. Notably, whereas some proteins are mobile on these membrane patches (*e.g.* monomeric $G\alpha_q$), others are not (*e.g.* GPCRs) (44). The advantages of this approach are the following: first, the absence of the cell autofluorescence improves PALM resolution for single molecule detection, and second, the elimination of most of the cytosolic components of the cell allows an analysis of receptor properties related to its plasma membrane environment, ideally reducing the receptor cluster origin to protein-protein and protein-lipid interactions present on the membrane. Notably, from fluorescence images, we still found actin filaments on these membrane patches (supplemental Fig. S6). On these structures, we observed that the β2 receptor was still clustered compared with the negative control and the clustering was lower compared with the whole fixed cell (Fig. 5).

DISCUSSION

The idea that signaling molecules, such as GPCRs, might be organized in oligomers or clusters is still a controversial topic, mostly because their visualization is precluded by the limited resolution power of conventional optics (~200 nm). By using PALM, we analyzed the clustering of the prototypical GPCR β2-adrenergic receptor, labeled with mEos2, in different cell lines such as HeLa, CHO, and H9C2. In HeLa cells, the receptors were randomly distributed all over the plasma membrane, and the clustering was negligible, similar to the negative control, even after a very short incubation with isoproterenol. Notably, when another GPCR, namely M3 muscarinic receptor, was analyzed or another cell line, such as CHO, was considered, receptor clustering was still not observed. Evidence of a GPCR not clustering in its basal state was also found in a recent study where, using TIRF microscopy, it was demonstrated that low-density M1 muscarinic receptors appear randomly distributed on the plasma membrane of CHO cells (9). Our evidence indicates that in these cell lines, receptor clustering is not required for GPCRs to be functional. In fact, in HeLa cells, even if there was no receptor clustering, the β2-adrenergic receptor was able to increase cAMP. However, considering that we looked for clusters of at least five molecules, we cannot exclude the presence of receptor oligomers in these conditions. During receptor internalization, we started to see an increase in receptor clustering that was enhanced by the addition of the inhibitor of the clathrin-dependent endocytosis, dynasore. The agonist-dependent internalization of the β2 receptor is known to be clathrin mediated (45), and we confirmed that receptor clusters during internalization corresponded to forming endosomes by colocalization experiments with clathrin-EGFP. Interestingly, considering that the β2 receptor has constitutive internalization through clathrin-independent endocytosis (46), the absence of clusters in the basal state may suggest a different number and size of forming endosomal structures that are used for clathrin-independent endocytosis compared with the clathrin-dependent one. Because our goal was to compare β2 receptor clustering in different cell types, we also considered cardiomyocytes, such

as H9C2 cells, derived from the embryonic rat heart, where the physiological role of the β2 receptor is well documented (31, 32). In addition, in this cell line, a very high degree of receptor clustering was reported by means of NSOM measurements (7, 15). When comparing the results from PALM with those from NSOM, the following considerations are taken into account. Whereas PALM is able to localize both isolated monomers as well as receptors being part of a cluster, NSOM sensitivity is limited to larger aggregates, lacking the ability to detect individual fluorophores on the plasma membrane. As a result, the real fraction of clustered molecules cannot be determined with NSOM. In H9C2 cells, the fraction of clustered receptors determined with PALM was about 10%. This indicates that, although the majority of the β2 receptors are randomly distributed on the plasma membrane, a small fraction of clusters is formed and can possibly have an important role in specific cellular plasma membrane compartments. A relevant finding emerging from our data is that the β2 receptor appears to form clusters in its basal condition only in H9C2 cells and not in HeLa or CHO, suggesting the importance of the cell type in determining multiprotein complexes. A possible explanation for this difference is that H9C2 cells, derived from the embryonic rat heart, compared with the other cells, express cell type-specific proteins responsible for receptor aggregation and/or have different plasma membrane composition. A recent paper (47) suggested that β2 receptor spatial confinement on the plasma membrane in H9C2 cells was mediated by two specific proteins that interact with the actin cytoskeleton, the ezrin-binding phosphoprotein EBP50 and the protein kinase A anchoring protein AKAP12. The appropriate expression of these two scaffolding proteins in H9C2 cells compared with other cell lines might be a possible explanation for our findings. We obtained a qualitative agreement with these results by performing single particle tracking PALM (48) measurements on living cells. Although the fast photobleaching of the fluorophore only allowed tracking for short times, we observed that the β2-mEos2 diffusion coefficient in H9C2 cells was lower than in HeLa cells (supplemental Fig. S7).

The presence of preassembled clusters in basal conditions prompted us to observe if different receptor ligands could affect protein clustering. Addition of the agonist isoproterenol for very short times did not significantly affect the β2 receptor assembly. These observations suggest that if this partial receptor clustered fraction in H9C2 is relevant in certain aspects for receptor signaling, this assembly is already preassociated before the addition of the ligand. It is also true that the receptor clustered fraction was not related to receptor basal activity because the inverse agonist ICI 118,551 did not affect cluster formation.

Considering that receptor clustering is a biological process related to the plasma membrane, we then decided to investigate the role of two main factors responsible for plasma membrane heterogeneity, namely cholesterol and the actin cytoskeleton. Both molecules have been shown in a different context to affect membrane protein properties (41–43), such as, for example, 5-hydroxytryptamine 1 receptor oligomerization (43). Interestingly, the sequestration of cholesterol induced by filipin or MβDC did not change the assembly of the β2 receptor, indicating that receptor clustering does not rely on lipid raft integrity, and thus ruling out the possibility that β2 cluster formation is associated with the raft. In a similar direction, Pontier *et al.* (8) have shown that the β2 receptor in HEK293 cells does not partition within the cholesterol-enrichment domain, and this is necessary to restrain receptor basal activity. To assess the role of the actin cytoskeleton, we treated H9C2 cells with the actin polymerization inhibitor cytochalasin D, which clearly reduced clustering of the β2 receptor. This implies an important role of the actin cytoskeleton in receptor assembly that is not associated with the lipid raft. To relate these observations in a physiological context, we tried the cAMP functional assay after actin depletion, but this alteration did not significantly affect the production of cAMP induced by the β2 receptor, as detected by bulk assay. In the near future, the use of novel functional approaches similar to those used for measuring the spatiotemporal dynamics of intracellular compartmentalized cAMP using FRET-based biosensors (49) may enable a more accurate analysis of the small differences in cAMP signaling in the plasma membrane cellular domains. The interaction between actin filaments and the β2 receptor is probably mediated by protein intermediates, as recently shown by Valentine and Haggie (47) for ezrin-binding phosphoprotein EBP50 and protein kinase A anchoring protein AKAP12. However, considering that other actin-binding proteins are relevant for GPCR-cytoskeleton interactions, *e.g.* filamin (24), we cannot rule out possible implications of other intermediates in β2 receptor-actin interactions. The relevance of the actin cytoskeleton was nicely confirmed in experiments based on functional supported cell-membrane sheets on poly-L-lysine-coated coverslips. Importantly, from fluorescence images, we still found actin filaments, even if decreased, present on the plasma membrane, implying a functional role of actin and its binding proteins in these membrane sheets. On these membrane patches, we found that the β2 receptor was still clustered compared with the negative control, and the fraction clustered was slightly decreased compared with the whole fixed cell.

In summary, we found that the prototypical GPCR β2-adrenergic receptor is partially preassociated in nanoscale-sized clusters only in the cardiomyocytes, such as H9C2 cells, but not in other cell lines, such as HeLa and CHO. Although cholesterol sequestration and removal did not affect receptor clustering, the inhibition of actin polymerization did decrease cluster formation. These findings suggest that receptor clustering is influenced by the actin cytoskeleton, but it does not rely on lipid raft integrity, thus ruling out the possibility that β2 receptor clusters are associated with the lipid raft. Scaffolding proteins present in H9C2 are most likely responsible for cell-specific receptor clustering mediated by actin filaments and the dynamics of this process have to be further investigated. This study has demonstrated how the application of PALM, combined with a careful choice of negative and positive controls, has suc-

cessfully allowed the quantitative determination of GPCR clusters compared with a randomly distributed peptide expressed on the plasma membrane of different cell types. The application of this powerful microscopy technique, as a quantitative tool, opens up the possibility to investigate and quantify the number of molecules in biological assemblies and determine the protein stoichiometry in signaling complexes.

Acknowledgments—We thank Dr. Vobornik (EPFL) and Dr. Julie Donaldson (NIH) for critical reading of our manuscript. We thank Dr. Gisou Van der Goot (EPFL), Dr. Laura Calzà (University of Bologna), Dr. Jurgen Wess (NIH), and Dr. Roberto Maggio (University of L'Aquila) for valuable discussion.

REFERENCES

1. Harding, A. S., and Hancock, J. F. (2008) Using plasma membrane nanoclusters to build better signaling circuits. *Trends Cell Biol.* **18,** 364–371
2. Manz, B. N., and Groves, J. T. (2010) Spatial organization and signal transduction at intercellular junctions. *Nat. Rev. Mol. Cell Biol.* **11,** 342–352
3. Bethani, I., Skånland, S. S., Dikic, I., and Acker-Palmer, A. (2010) Spatial organization of transmembrane receptor signaling. *EMBO J.* **29,** 2677–2688
4. Patel, H. H., Murray, F., and Insel, P. A. (2008) G-protein-coupled receptor-signaling components in membrane raft and caveolae microdomains. *Handb. Exp. Pharmacol.* **186,** 167–184
5. Jacobson, K., Mouritsen, O. G., and Anderson, R. G. (2007) Lipid rafts, at a crossroad between cell biology and physics. *Nat. Cell Biol.* **9,** 7–14
6. Allen, J. A., Halverson-Tamboli, R. A., and Rasenick, M. M. (2007) Lipid raft microdomains and neurotransmitter signaling. *Nat. Rev. Neurosci.* **8,** 128–140
7. Ianoul, A., Grant, D. D., Rouleau, Y., Bani-Yaghoub, M., Johnston, L. J., and Pezacki, J. P. (2005) Imaging nanometer domains of β-adrenergic receptor complexes on the surface of cardiac myocytes. *Nat. Chem. Biol.* **1,** 196–202
8. Pontier, S. M., Percherancier, Y., Galandrin, S., Breit, A., Galés, C., and Bouvier, M. (2008) Cholesterol-dependent separation of the β2-adrenergic receptor from its partners determines signaling efficacy. Insight into nanoscale organization of signal transduction. *J. Biol. Chem.* **283,** 24659–24672
9. Hern, J. A., Baig, A. H., Mashanov, G. I., Birdsall, B., Corrie, J. E., Lazareno, S., Molloy, J. E., and Birdsall, N. J. (2010) Formation and dissociation of M1 muscarinic receptor dimers seen by total internal reflection fluorescence imaging of single molecules. *Proc. Natl. Acad. Sci. U.S.A.* **107,** 2693–2698
10. Powell, R. D., Halsey, C. M., and Hainfeld, J. F. (1998) Combined fluorescent and gold immunoprobes. Reagents and methods for correlative light and electron microscopy. *Microsc. Res. Tech.* **42,** 2–12
11. Betzig, E., Patterson, G. H., Sougrat, R., Lindwasser, O. W., Olenych, S., Bonifacino, J. S., Davidson, M. W., Lippincott-Schwartz, J., and Hess, H. F. (2006) Imaging intracellular fluorescent proteins at nanometer resolution. *Science* **313,** 1642–1645
12. Lippincott-Schwartz, J., and Patterson, G. H. (2009) Photoactivatable fluorescent proteins for diffraction-limited and super-resolution imaging. *Trends Cell Biol.* **19,** 555–565
13. Fotiadis, D., Scheuring, S., Müller, S. A., Engel, A., and Müller, D. J. (2002) Imaging and manipulation of biological structures with the AFM. *Micron* **33,** 385–397
14. Liang, Y., Fotiadis, D., Filipek, S., Saperstein, D. A., Palczewski, K., and Engel, A. (2003) Organization of the G protein-coupled receptors rhodopsin and opsin in native membranes. *J. Biol. Chem.* **278,** 21655–21662
15. Vobornik, D., Rouleau, Y., Haley, J., Bani-Yaghoub, M., Taylor, R., Johnston, L. J., and Pezacki, J. P. (2009) Nanoscale organization of β2-adrenergic receptor-Venus fusion protein domains on the surface of mammalian cells. *Biochem. Biophys. Res. Commun.* **382,** 85–90
16. Tanaka, K. A., Suzuki, K. G., Shirai, Y. M., Shibutani, S. T., Miyahara, M. S., Tsuboi, H., Yahara, M., Yoshimura, A., Mayor, S., Fujiwara, T. K., and Kusumi, A. (2010) Membrane molecules mobile even after chemical fixation. *Nature Methods* **7,** 865–866
17. Annibale, P., Vanni, S., Scarselli, M., Rothlisberger, U., and Radenovic, A. (2011) Identification of clustering artifacts in photoactivated localization microscopy. *Nat. Methods* **8,** 7
18. McKinney, S. A., Murphy, C. S., Hazelwood, K. L., Davidson, M. W., and Looger, L. L. (2009) A bright and photostable photoconvertible fluorescent protein. *Nat. Methods* **6,** 131–133
19. Annibale, P., Vanni, S., Scarselli, M., Rothlisberger, U., and Radenovic, A. (2011) Quantitative photoactivated localization microscopy. Unraveling the effects of photoblinking. *Plos One* **6,** e22678
20. Chichili, G. R., and Rodgers, W. (2007) Clustering of membrane raft proteins by the actin cytoskeleton. *J. Biol. Chem.* **282,** 36682–36691
21. Perez, J. B., Martinez, K. L., Segura, J. M., and Vogel, H. (2006) Supported cell-membrane sheets for functional fluorescence imaging of membrane proteins. *Adv. Funct. Materials* **16,** 306–312
22. Shroff, H., White, H., and Betzig, E. (2008) Photoactivated localization microscopy (PALM) of adhesion complexes. *Curr. Protoc. Cell Biol.* Chapter 4, Unit 4 21
23. Diggle, P. J. (ed) (2003) *Statistical Analyisis of Spatial Point Patterns,* Arnold, London
24. Lin, R., Karpa, K., Kabbani, N., Goldman-Rakic, P., and Levenson, R. (2001) Dopamine D2 and D3 receptors are linked to the actin cytoskeleton via interaction with filamin A. *Proc. Natl. Acad. Sci. U.S.A.* **98,** 5258–5263
25. Puthenveedu, M. A., and von Zastrow, M. (2006) Cargo regulates clathrin-coated pit dynamics. *Cell* **127,** 113–124
26. Haase, P. (1995) Spatial pattern analysis in ecology based on Ripley's K-function: Introduction and methods of edge correction. *J. Vegetation Sci.* **6,** 575–582
27. Flesch, M., Ettelbrück, S., Rosenkranz, S., Maack, C., Cremers, B., Schlüter, K. D., Zolk, O., and Böhm, M. (2001) Differential effects of carvedilol and metoprolol on isoprenaline-induced changes in β-adrenoceptor density and systolic function in rat cardiac myocytes. *Cardiovasc. Res* **49,** 371–380
28. Hegener, O., Prenner, L., Runkel, F., Baader, S. L., Kappler, J., and Häberlein, H. (2004) Dynamics of β2-adrenergic receptor-ligand complexes on living cells. *Biochemistry* **43,** 6190–6199
29. Samama, P., Cotecchia, S., Costa, T., and Lefkowitz, R. J. (1993) A mutation-induced activated state of the β2-adrenergic receptor. Extending the ternary complex model. *J. Biol. Chem.* **268,** 4625–4636
30. Kassis, S., Henneberry, R. C., and Fishman, P. H. (1984) Induction of catecholamine-responsive adenylate cyclase in HeLa cells by sodium butyrate. Evidence for a more efficient stimulatory regulatory component. *J. Biol. Chem.* **259,** 4910–4916
31. Yano, N., Suzuki, D., Endoh, M., Tseng, A., Stabila, J. P., McGonnigal B. G., Zhao, T. C., Padbury, J. F., and Tseng, Y. T. (2008) β-Adrenergic receptor mediated protection against doxorubicin-induced apoptosis in cardiomyocytes. The impact of high ambient glucose. *Endocrinology* **149,** 6449–6461
32. Hescheler, J., Meyer, R., Plant, S., Krautwurst, D., Rosenthal, W., and Schultz, G. (1991) Morphological, biochemical, and electrophysiological characterization of a clonal cell (H9c2) line from rat heart. *Circ. Res.* **69,** 1476–1486
33. Hothersall, J. D., Black, J., Caddick, S., Vinter, J. G., Tinker, A., and Baker, J. R. (2011) The design, synthesis, and pharmacological characterization of novel β2-adrenoceptor antagonists. *Br. J. Pharmacol.* **164,** 2
34. Collins, J. J., and Phillips, M. C. (1982) The stability and structure of cholesterol-rich codispersions of cholesterol and phosphatidylcholine. *J. Lipid Res.* **23,** 291–298
35. Lingwood, D., and Simons, K. (2010) Lipid rafts as a membrane-organizing principle. *Science* **327,** 46–50
36. Paila, Y. D., and Chattopadhyay, A. (2010) Membrane cholesterol in the function and organization of G-protein coupled receptors. *Subcell. Biochem.* **51,** 439–466
37. Awasthi-Kalia, M., Schnetkamp, P. P., and Deans, J. P. (2001) Differential effects of filipin and methyl-β-cyclodextrin on B cell receptor signaling. *Biochem. Biophys. Res. Commun.* **287,** 77–82
38. Naslavsky, N., Weigert, R., and Donaldson, J. G. (2004) Characterization of

a nonclathrin endocytic pathway. Membrane cargo and lipid requirements. *Mol. Biol. Cell* **15,** 3542–3552
39. Kenworthy, A. K., Nichols, B. J., Remmert, C. L., Hendrix, G. M., Kumar, M., Zimmerberg, J., and Lippincott-Schwartz, J. (2004) Dynamics of putative raft-associated proteins at the cell surface. *J. Cell Biol.* **165,** 735–746
40. Kwik, J., Boyle, S., Fooksman, D., Margolis, L., Sheetz, M. P., and Edidin, M. (2003) Membrane cholesterol, lateral mobility, and the phosphatidylinositol 4,5-bisphosphate-dependent organization of cell actin. *Proc. Natl. Acad. Sci. U.S.A.* **100,** 13964–13969
41. Ganguly, S., Pucadyil, T. J., and Chattopadhyay, A. (2008) Actin cytoskeleton-dependent dynamics of the human serotonin1A receptor correlates with receptor signaling. *Biophys. J.* **95,** 451–463
42. Ganguly, S., and Chattopadhyay, A. (2010) Cholesterol depletion mimics the effect of cytoskeletal destabilization on membrane dynamics of the serotonin1A receptor. A zFCS study. *Biophys. J.* **99,** 1397–1407
43. Ganguly, S., Clayton, A. H., and Chattopadhyay, A. (2011) Organization of higher-order oligomers of the serotonin1(A) receptor explored utilizing homo-FRET in live cells. *Biophys. J.* **100,** 361–368
44. Perez, J. B., Segura, J. M., Abankwa, D., Piguet, J., Martinez, K. L., and Vogel, H. (2006) Monitoring the diffusion of single heterotrimeric G proteins in supported cell-membrane sheets reveals their partitioning into microdomains. *J. Mol. Biol.* **363,** 918–930
45. Hanyaloglu, A. C., and von Zastrow, M. (2008) Regulation of GPCRs by endocytic membrane trafficking and its potential implications. *Annu. Rev. Pharmacol. Toxicol.* **48,** 537–568
46. Scarselli, M., and Donaldson, J. G. (2009) Constitutive internalization of G protein-coupled receptors and G proteins via clathrin-independent endocytosis. *J. Biol. Chem.* **284,** 3577–3585
47. Valentine, C. D., and Haggie, P. M. (2011) Confinement of β1- and β2-adrenergic receptors in the plasma membrane of cardiomyocyte-like H9c2 cells is mediated by selective interactions with PDZ domain and A-kinase anchoring proteins but not caveolae. *Mol. Biol. Cell* **22,** 2970–2982
48. Manley, S., Gillette, J. M., Patterson, G. H., Shroff, H., Hess, H. F., Betzig, E., and Lippincott-Schwartz, J. (2008) High-density mapping of single-molecule trajectories with photoactivated localization microscopy. *Nat. Methods* **5,** 155–157
49. Gesellchen, F., Stangherlin, A., Surdo, N., Terrin, A., Zoccarato, A., Zaccolo, M. (2011) Measuring spatiotemporal dynamics of cyclic AMP signaling in real-time using FRET-based biosensors. *Methods Mol. Biol.* **746,** 297–316